Journal of Volcanology and Geothermal Research 181 (2009) 207–218

Contents lists available at ScienceDirect

Journal of Volcanology and Geothermal Research

journal homepage: www.elsevier.com/locate/jvolgeores

Ground deformation patterns at White Island volcano (New Zealand) between 1967 and 2008 deduced from levelling data

Aline Peltier [a,b,*], Bradley Scott [c], Tony Hurst [a]

[a] GNS Science, Lower Hutt, New Zealand
[b] Institut de Physique du Globe de Paris, Paris, France
[c] GNS Science, Taupo, New Zealand

ARTICLE INFO

Article history:
Received 7 August 2008
Accepted 9 January 2009
Available online 30 January 2009

Keywords:
White Island
levelling measurement
numerical modelling
vertical deformation
magma injection
hydrothermal circulation

ABSTRACT

Since 1967, levelling measurements have been conducted in the main crater of White Island volcano. Interpretation of these data using numerical modelling reveals that shallow pressure sources (200–600 m deep) extending up to the subsurface dominated the long-term deformation pattern consisting of inflation/deflation cycles. The time sequence of height changes, magnetic changes, and fumarole temperature and chemistry reveal that surface changes were caused by increasing temperature below the main crater, reflecting the presence of magma at shallow depth. The uplift and subsidence are interpreted in terms of increase or decrease in fluid pore pressure in response to changes of the heat and gas flux. The subsidence during and following eruptions could be also linked with removal of material at depth to feed the eruptions.

1. Introduction

For several decades, ground deformation studies in volcanic area have provided useful information to enable eruption forecasts and to constrain the shape and the evolution of volcano plumbing systems with time (Dvorak and Dzurisin, 1997; Dzurisin, 2003). At White Island (New Zealand), the monitoring of vertical deformation has been conducted since 1967 by periodic levelling surveys of the Main Crater floor. Changes in the levels of the crater floor and their relation to the eruptive activity have been previously described for the 1967–1982 period by Clark (1973, 1982) and Clark and Otway (1989) but the origin of the ground deformation is poorly known. The active role of hydrothermal systems in the dynamics of ground deformation has been recently highlighted in several volcanoes worldwide, such as Campi Flegrei (Gottsmann et al., 2006) and Yellowstone (Dzurisin et al., 1994; Wicks et al., 1998). White Island is characterized both by strong hydrothermal and magmatic activity, and ground deformation induced by these two activities must be distinguished in order to better forecast eruptions in the future. Compilation of a large database over 40 years allows us to make a precise analysis of the long-term ground deformation pattern. The aim of this paper is to constrain the sources of ground deformation at White Island between 1967 and 2008 through numerical modelling inversions in order to understand the relationship between ground deformation, eruptive activity and hydrothermal circulations.

2. Geological setting

White Island is an offshore andesitic composite volcano located about 50 km from the Bay of Plenty coast (North Island of New Zealand, Fig. 1A). It lies at the north-eastern end of the Taupo Volcanic Zone, a zone of crustal thinning and extension located above the oblique subduction of the Pacific plate beneath the Australian plate. A main crater divided into three sub-craters (eastern, central and western sub-craters) occupies the eastern end of the Island (Figs. 1B and 2). Historic activity is concentrated in the western half of this crater (Fig. 1) and is characterized by continuous sulphur and fumarolic gas emissions and intermittent minor phreatic, phreato-magmatic and magmatic eruptions (Clark, 1973; Cole and Nairn, 1975). During the last 40 years, a variety of eruptions have occurred. Most eruptions are dominantly phreatic and phreatomagmatic and emitted very small volumes of eruptive products, around 10^6–10^7 m^3. The large eruptive sequences of 1976–1982 and 1986–1994 led progressively to the formation of a collapse crater complex in the western sub-crater (Fig. 2B), which has been partly filled by an acid lake since February 2003. Previous studies suggest that magma feeding these eruptions probably originated from reservoirs located at shallow depths of around 500 m below sea level (Houghton and Nairn, 1989; Cole et al., 2000). Two other deeper reservoirs, located at depths of 1–2 km and 2–7 km, respectively, have been highlighted

* Corresponding author. Present address: Institut de Physique du Globe de Paris, CNRS, UMR 7154-Géologie des Systèmes Volcaniques, 4 place jussieu, Paris, France. Tel.: +33 1 44 27 25 06; fax: +33 1 44 27 73 85.
E-mail addresses: peltier@ipgp.jussieu.fr (A. Peltier), b.scott@gns.cri.nz (B. Scott), t.hurst@gns.cri.nz (T. Hurst).

0377-0273/$ – see front matter © 2009 Elsevier B.V. All rights reserved.
doi:10.1016/j.jvolgeores.2009.01.020

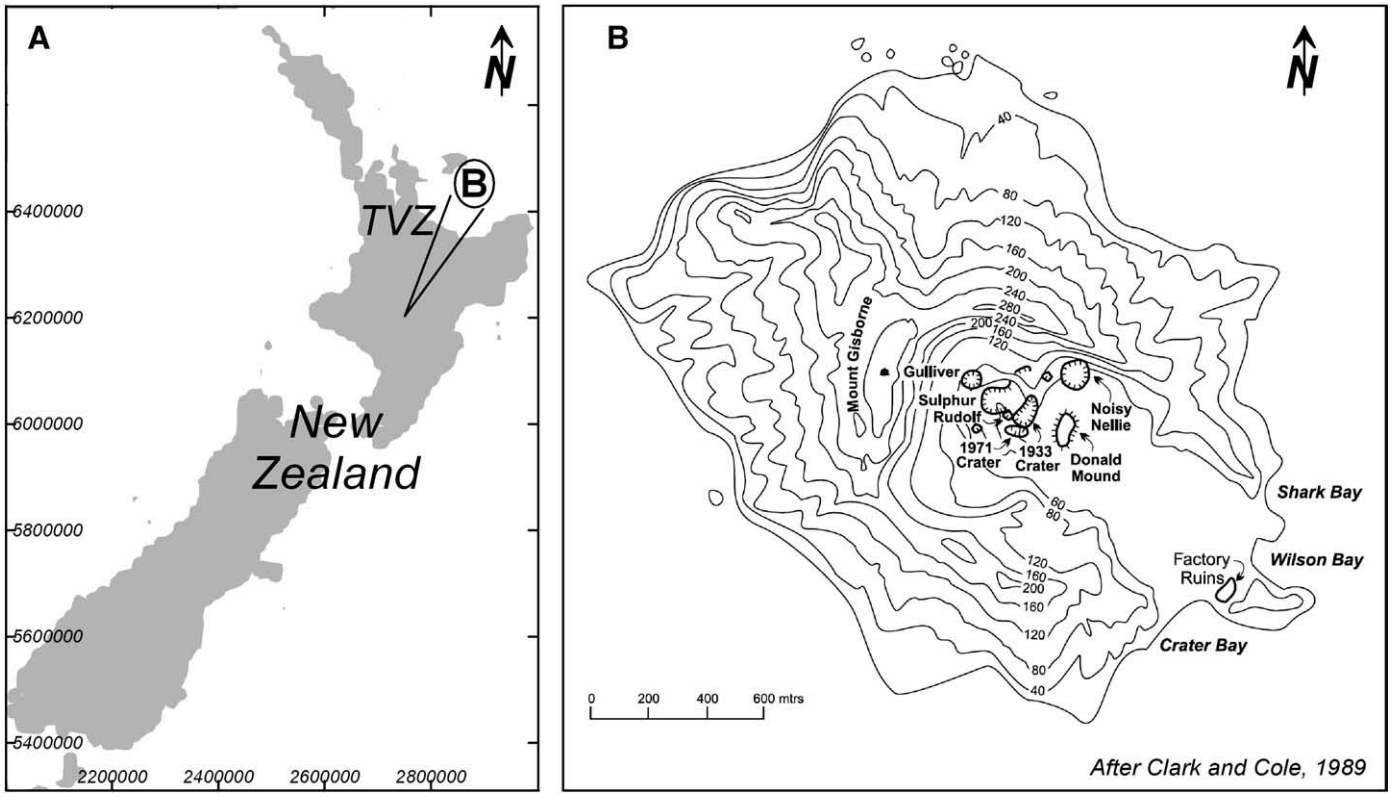

Fig. 1. (A) Location of the Taupo Volcanic Zone (TVZ, delimited by black lines) and White Island (circle). (B) Topography of White Island and location of the main structures (after Clark and Cole, 1989). Coordinates are in New Zealand Map Grid Projection (metres).

by geochemical studies (Houghton and Nairn, 1989; Cole et al., 2000). An active hydrothermal system, expressed at the surface by areas of steaming ground, hot springs and fumaroles, lies below the main crater (Giggenbach et al., 1989). Volcano-tectonic earthquakes mainly originate in the hydrothermal area at very shallow depths (<1 km) beneath the central and eastern sub-craters of the main crater (Nishi et al., 1996b). Nishi et al. (1996b) interpreted the shallow earthquakes to result from rapid changes in pore fluid pressure.

3. Levelling data

3.1. Survey method

Since 1967, periodic (3–4 times per year) levelling surveys have been conducted across accessible portions of the main crater floor to monitor relative vertical displacements (Fig. 2A, B). Currently these vertical displacements are measured at 22 sites located on the main crater floor (Fig. 2B). The site numbering system was changed in 1993.

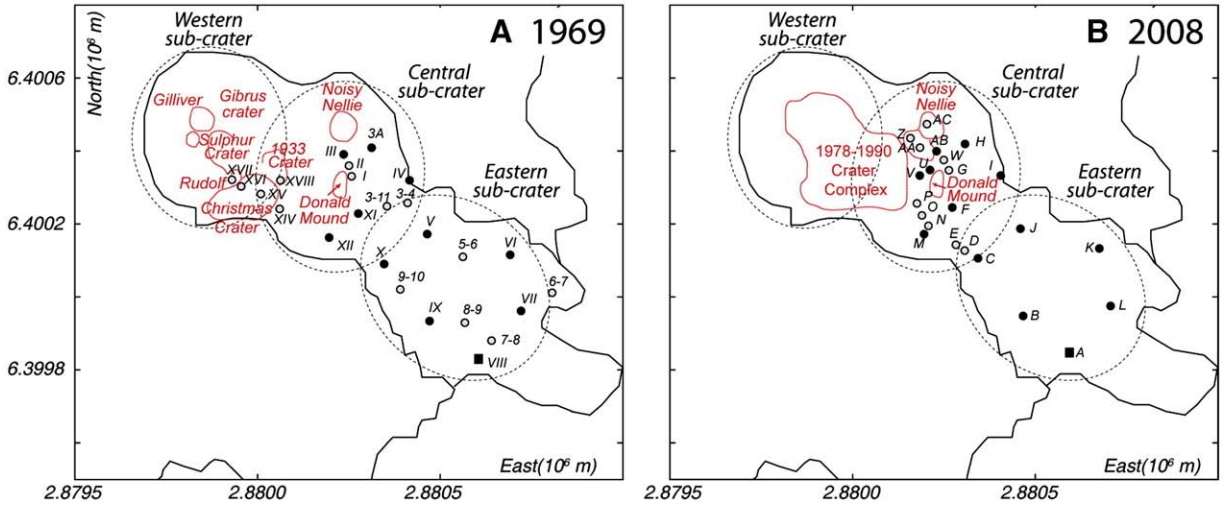

Fig. 2. Location of levelling sites inside the White Island main crater in (A) 1969 and in (B) 2008. Squares represent the origin (VIII and A), filled and open circles represent the sites common and not common for the two periods, respectively. Dashed circles and bold red contour underlined the sub-craters and the crater boundaries, respectively. Note that in 1993 peg identification changed. (For interpretation of the references to color in this figure legend, the reader is referred to the web version of this article.)

Over the 40 years of level monitoring, significant topographical changes have occurred within the main crater due to eruptive activity and formation of collapse craters (Fig. 2A, B) and these sometimes led to the destruction of pegs, disrupting the continuity of measurements at many sites (Figs. 2 and 3). In particular, the pegs located in the western part of the network (XV, XVI, XVII) were destroyed and engulfed into Christmas Crater in early 1977.

The estimated standard deviation for a typical survey ranges from 2–5 mm and is directly proportional to the distance of each peg from the origin, peg A, which is located in the south-eastern part of the

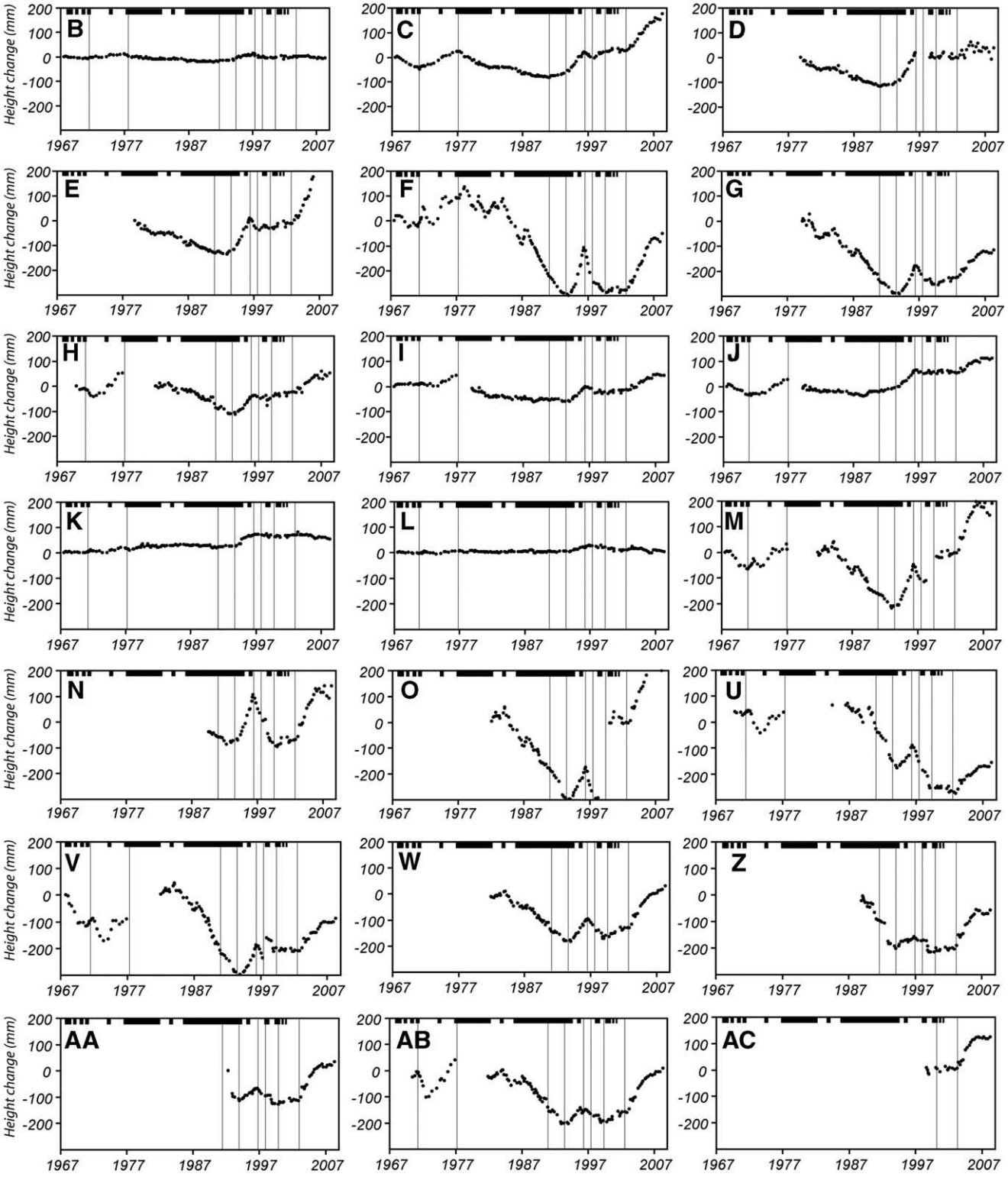

Fig. 3. Height changes (mm) relative to the origin, A, (see Fig. 2B for location) recorded on each peg between July 1967 and April 2008 at White Island. The lines highlight changes in the global deformation trend. Eruptive periods are highlighted by black lines at the top of each chart.

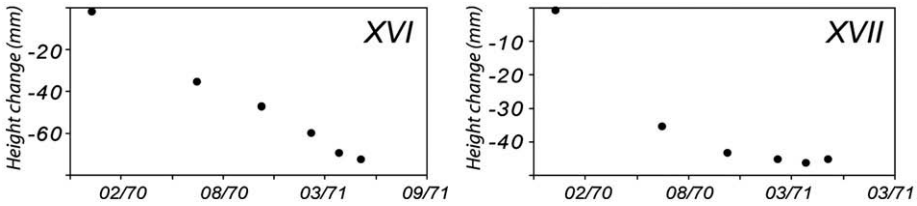

Fig. 4. Height changes (mm) relative to the origin (VIII, see Fig. 2A for location) recorded on pegs XVI and XVII located inside the 1933 crater between 1969 and 1971. The measurements between 1971 and 1976 are discontinuous and not reported in this figure.

network (see Fig. 2B for location; Scott, 1992). No measurement has been made at White Island to constrain horizontal deformation.

3.2. Vertical deformation evolution between 1967 and 2008

The levelling data from the pegs not destroyed by the 1976–1982 and 1986–1994 eruptive sequences are plotted in Figs. 3 and 4 in the form of apparent height changes relative to the origin, peg A. Short-term disturbances are visible at many sites, however we recognise eight long-term episodes of deformation between 1967 and 2008: (1) July 1967–April 1971, (2) April 1971–December 1976, (3) December 1976–November 1990, (4) November 1990–January 1994, (5) January 1994–May 1996, (6) May 1996–December 1997, (7) December 1997–February 2000 and (8) November 2002–May 2008. Between 2000 and 2002, vertical deformation was weak and no clear trend can be highlighted (Fig. 3). To visualize the pattern and the distribution of vertical deformation, the average rate of vertical displacement relative to the origin, peg A, is shown for the eight selected periods in Fig. 5.

3.2.1. July 1967–April 1971

Between July 1967 and April 1971, the major ground deformation signal was a subsidence centred to the west of the network (maximum rates of 0.03–0.04 m yr^{-1}) (Figs. 3 and 5). The installation of pegs inside the 1933 crater in December 1969 revealed that the greatest subsidence occurred inside the 1933 Crater (0.05 m yr^{-1}) (Figs. 4 and 5). Note that a short-term broad asymmetric uplift was recorded at the first re-level, in November 1967, with a maximum rate of 0.07 m yr^{-1} near Donald Mound (F on Fig. 3). This uplift preceded an episode of eruptive activity inside the Rudolf vent (Clark, 1970). During this period, Rudolf fumarole (on the back wall of the 1933 crater) developed into an active vent with the occurrence of intermittent ash eruptions: January 27th 1968–February 1969, August–September 1969 and June 1970. The main phase of ash eruption inside the Rudolf vent was in February 1968 (Clark, 1970).

3.2.2. April 1971–December 1976

In April 1971, the signal reversed at all sites highlighting an uplift of the central sub-crater relative to the origin (Figs. 3 and 5). The highest uplift was recorded around Donald Mound, with a mean rate of 0.03–0.04 m yr^{-1}. Three eruptions occurred during this period and disturbed the long-term pattern: April 1971 (Noisy Nellie Crater), 19–20 July 1971 (South of Rudolf crater) and September 1974 (south-east of Donald Mound). After each of these eruptions a slight short-term subsidence of the crater floor was recorded on pegs F, H, V, M, U, and AB before uplift centred below Donald Mound started again (Fig. 3).

3.2.3. December 1976–November 1990

From December 1976 to November 1990, the most significant deformation signal was a subsidence of the central sub-crater floor. The largest deformation rates of 0.02 m yr^{-1} were measured at pegs F and G (Figs. 3 and 5). Over this period, the long-term subsidence was centred near eruptive vents that developed west of the monitored network. Superimposed on the long-term subsidence, short-term episodes of uplift and subsidence were recorded on sites F, G and H with peaks visible in March 1978, May 1980, November 1982, February 1984 and June 1987 (Fig. 3).

This more or less continuous subsidence corresponds to a period of quasi continuous eruptive activity marking the largest historic eruptions. During this period many collapse craters, including Christmas, Gibrus and 1978 craters, were formed during cyclic eruptive sequences (Houghton and Nairn, 1989). Localized inflation centred near the Donald Mound preceded or accompanied the resurgences of eruptive activity during this period. For instance, the rising signal at sites F, G and H in 1987 occurred before the first explosive eruption of a renewed cycle of activity at that time.

3.2.4. November 1990–January 1994

The crater subsidence recorded between 1976 and 1990 was interrupted after November 1990. Two signals became apparent within the monitored area; both uplift and subsidence were recorded until January 1994. Sites located in the middle of the network (B, C, D, J) recorded an uplift relative to the origin (maximum rate of 0.008 m yr^{-1} on site C), whereas the sites located to the west (E, F, G, H, I, M) recorded a subsidence (0.01 to 0.03 m yr^{-1}) (Figs. 3 and 5). The eruptive sequence which began in 1986 continued during this period, with notably the formation of a new crater collapse in 1990 (enlargement of the 1978–1990 Crater Complex).

3.2.5. January 1994–May 1996

After January 1994 the deformation signal reversed at sites located to the west and increased on the sites to the east revealing a crater wide uplift relative to the origin, with a maximum rise recorded on sites F and M (0.08 m yr^{-1} and 0.07 m yr^{-1}, respectively, Figs. 3 and 5). This period corresponds to the end of the eruptive sequence of 1976–1994 (in July). Minor eruptions occurred on 28–29 June, 1995 but did not disturb the deformation behaviour and the global inflation of the central sub-crater continued until May 1996.

3.2.6. May 1996–December 1997

In May 1996, a reversal of the previous trend occurred with a drop recorded at all sites (Figs. 3 and 5). The maximum subsidence rate of 0.09 m yr^{-1} was recorded on peg F. No eruptive activity occurred over this period.

3.2.7. December 1997–February 2000

Between December 1997 and February 2000, the sites located at the west of the network continued to record a strong subsidence (maximum rate of 0.04 m yr^{-1} on peg N) whereas at the same time an inflation centred on site C was recorded (Figs. 3 and 5).

During this period minor explosive eruptions, ash emissions and crater formation continued from 1978/1990 Crater Complex. The largest magmatic eruption of the 1976–2000 period occurred in July 2000, marking the end of the eruptive episode.

3.2.8. November 2002–May 2008

After November 2002, a deformation signal characterized by a strong uplift at the western sites became established and continued until at least April 2008. The main uplift was centred in the western crater around sites F, M, N and O (rates of 0.04–0.05 m yr^{-1}, Figs. 3 and 5) with two other small signals near pegs C and AA–AB. By contrast levelling points furthest to the east were characterized by no significant changes or a slight subsidence relative to peg A. No eruptive activity was noted over this period but the greatest uplift occurred at the same time as a crater lake became established inside the 1978/1990 Crater Complex in

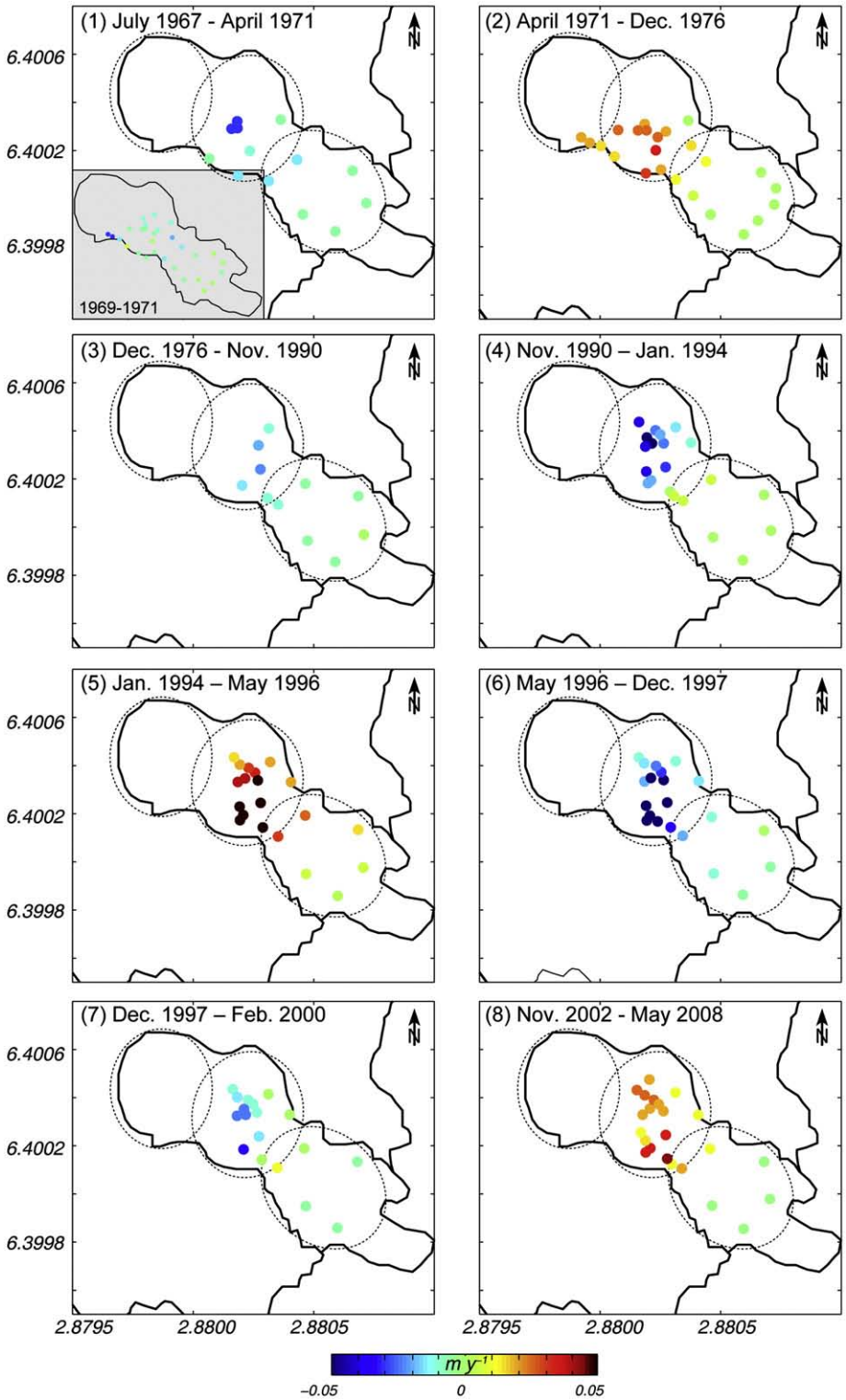

Fig. 5. Average vertical deformation rates relative to the origin, peg A, (in m yr^{-1}) for the eight separate periods: (1) July 1967–April 1971, (2) April 1971–December 1976, (3) December 1976–November 1990, (4) November 1990–January 1994, (5) January 1994–May 1996, (6) May 1996–December 1997, (7) December 1997–February 2000 and (8) November 2002–May 2008. Coordinates are in New Zealand Map Grid Projection (10^6 m). (For interpretation of the references to color in this figure legend, the reader is referred to the web version of this article.)

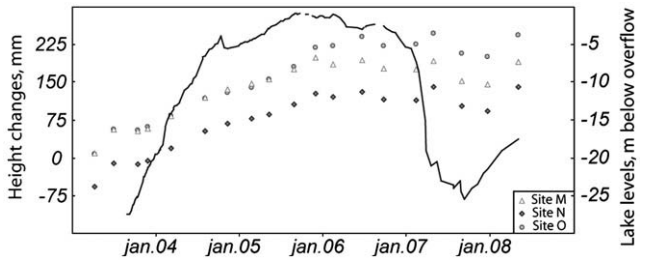

Fig. 6. Comparison between the height changes recorded on sites M, N, O and the Crater Lake levels (solid line) between 2003 and 2008.

February 2003 (Fig. 6; Scott et al., 2004). Fumarole activity also increased in the area of pegs C, D and E.

4. Comparison of levelling data with magnetic changes, fumarole temperature and fumarole chemistry

4.1. Magnetic changes

Christoffel (1989), Hurst and Christoffel (1973) and Hurst et al. (2004) noted an anti-correlation between the short-term height level changes and the magnetic changes. These authors observed changes of several hundred nanoTesla over periods of months to years at points on the crater floor, with drops in the magnetic field strength corresponding to ground level rises and vice-versa. This inverse correlation is expected when both height level and magnetic changes are due to temperature fluctuations. A rise of temperature at depth would affect the magnetic field if rock temperatures were in the range of 350–600 °C and thus approaching or reaching the Curie point temperature which produces total thermal demagnetisation (Hurst et al., 2004). The long-term subsidence recorded in 1990–1994, do not seem to be correlated with magnetic changes (Hurst et al., 2004). Hurst et al. (2004) suggested that this might reflect the sensitivity of the level monitoring to slow processes such a loss of fluid from the hydrothermal system or sagging of ground into the large collapse craters, which do not directly affect the magnetic measurements.

4.2. Fumarole temperature

A good temporal correlation is observed between peaks of fumarole maximum temperature at Donald Mound and uplift of the nearby sites (Fig. 7A). During the eruptive sequences of 1976–1982 and 1986–1994, the short term inflation linked with resurgence of surface activity was immediately followed by strong deflation, with declining temperatures and surface activity (Fig. 7A).

4.3. Fumarole chemistry

Fig. 7B, C, D, E compares the concentration of HCl, S, CO_2 and N_2 in the fumaroles of the Donald Mound area with the height change at site F over the 1971–1997 period. At low temperatures, hydrochloric acid (HCl) and sulphur gases react with the rocks and a smaller proportion of these gases reach the surface. CO_2 and N_2 are less reactive gases, so their concentrations in fumaroles are more closely related to the amount of these gases released from magma. A good correlation between HCl and S concentrations and the height changes is observed until 1978. After 1978, HCl and S concentrations and the height changes were anti-correlated (peak of S corresponding to low height level). During the energetic eruptive sequence of 1976–1982, the underground hydrothermal system was disturbed by the formation of collapse craters west of Donald Mound. After these changes, HCl and S were in much lower concentrations than during the 1971–1980 period. During the 1971–1976 period, peaks of HCl and S were preceded a few months earlier by peaks of CO_2 and N_2 which reacted less with the rocks, whereas during the 1976–1984 period the peaks of S, HCl, CO_2 and N_2 were coincident, indicating gas flux via the open eruptive vents.

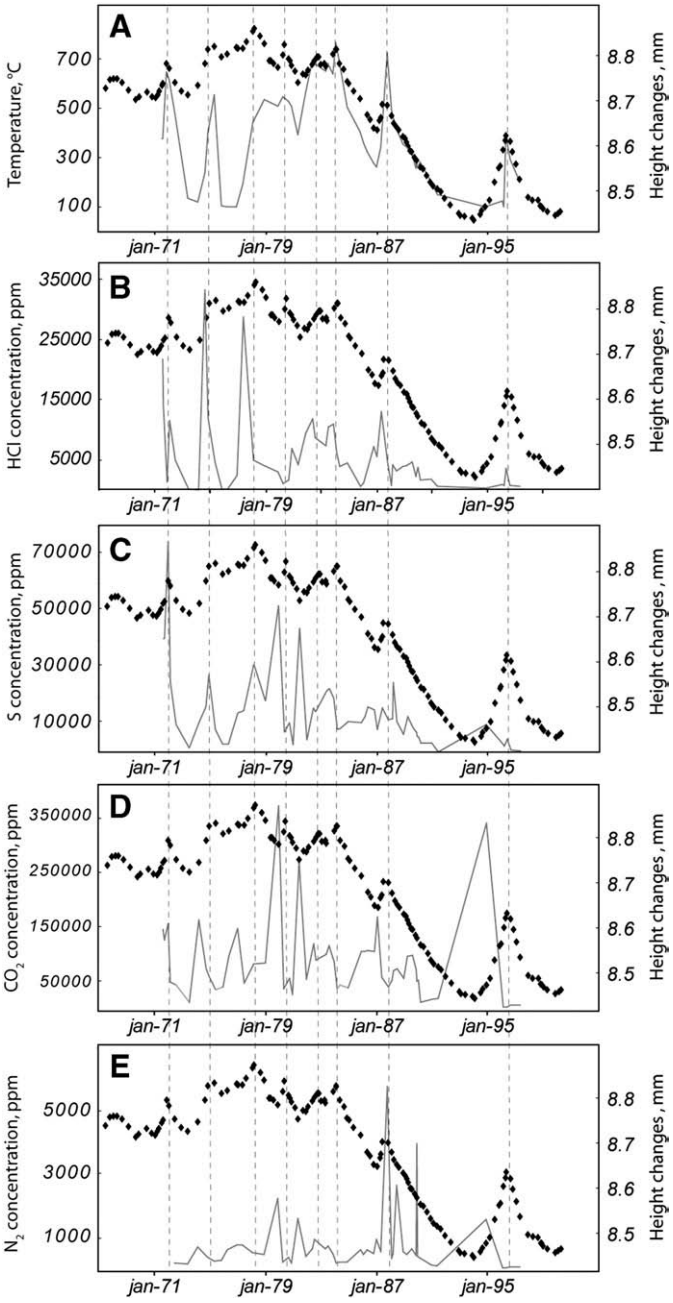

Fig. 7. Comparison between the height changes recorded on site F (black) relative to the origin and (A) the temperature at Donald Mound, (B) HCl, (C) S, (D) CO_2 and (E) N_2 gas concentrations in Donald Mound fumaroles (grey). HCl, S, CO_2 and N_2 data are from Giggenbach and Sheppard (1989) and Bruce Christenson (personal communication). Dashed lines represent the peaks of uplift on site F.

Fig. 8. Location and geometry of the pressure sources modelled for the eight periods: (1, blue) July 1967–April 1971, (2, green) April 1971–December 1976, (3, red) December 1976–November 1990, (4, black) November 1990–January 1994, (5, orange) January 1994–May 1996, (6; grey) May 1996–December 1997, (7, purple) December 1997–February 2000 and (8, brown) November 2002–May 2008. (For interpretation of the references to color in this figure legend, the reader is referred to the web version of this article.)

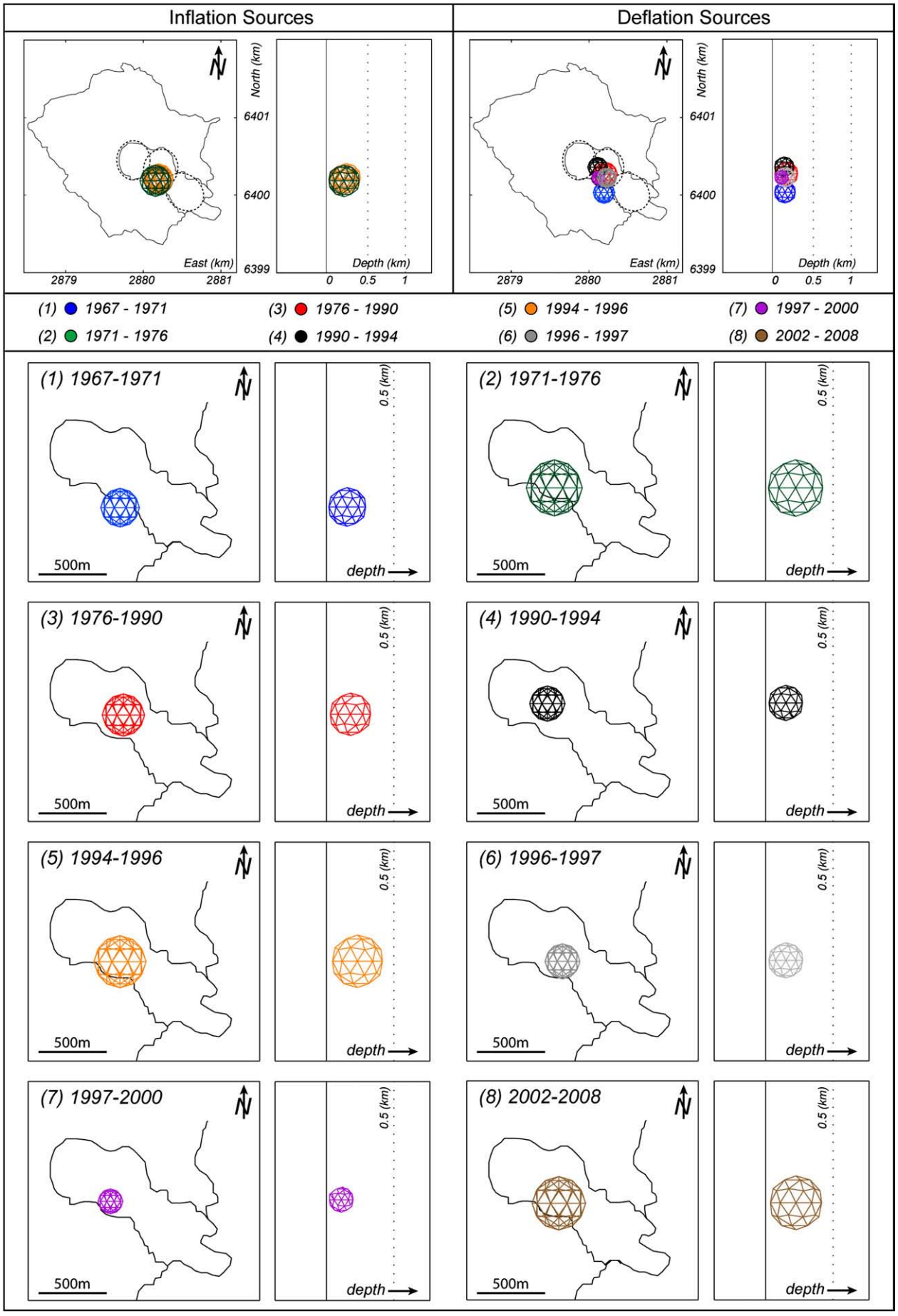
Inflation Sources
Deflation Sources
North (km)
6401
6400
6399
East (km)
2879
2880
2881
Depth (km)
0
0.5
1
(1) 1967 - 1971
(2) 1971 - 1976
(3) 1976 - 1990
(4) 1990 - 1994
(5) 1994 - 1996
(6) 1996 - 1997
(7) 1997 - 2000
(8) 2002 - 2008
(1) 1967-1971
(2) 1971-1976
(3) 1976-1990
(4) 1990-1994
(5) 1994-1996
(6) 1996-1997
(7) 1997-2000
(8) 2002-2008
500m
0.5 (km)
depth

5. Numerical modelling

5.1. Inversion and method

Levelling data was inverted using numerical modelling to constrain source locations that could account for the deformation patterns observed during the successive periods of crater floor uplifts and subsidences. We used the vertical displacements of the pegs obtained by subtracting the initial displacement from the final one during each defined time periods. Vertical displacements are used as data input in a 3D elastic model, Mc3f, based on a mixed boundary element method (Cayol, 1996; Cayol and Cornet, 1997). The model is combined with Sambridge's Monte Carlo inversion method (Sambridge, 1999) to minimize the misfit function (Fukushima et al., 2005), i.e. the normalized root mean square error between calculated and observed displacements. For the calculation, the medium is assumed to be elastic, homogeneous and isotropic (Cayol, 1996; Cayol and Cornet, 1997), with a Young's modulus of 30 GPa, and a Poisson's ratio of 0.25. The structures

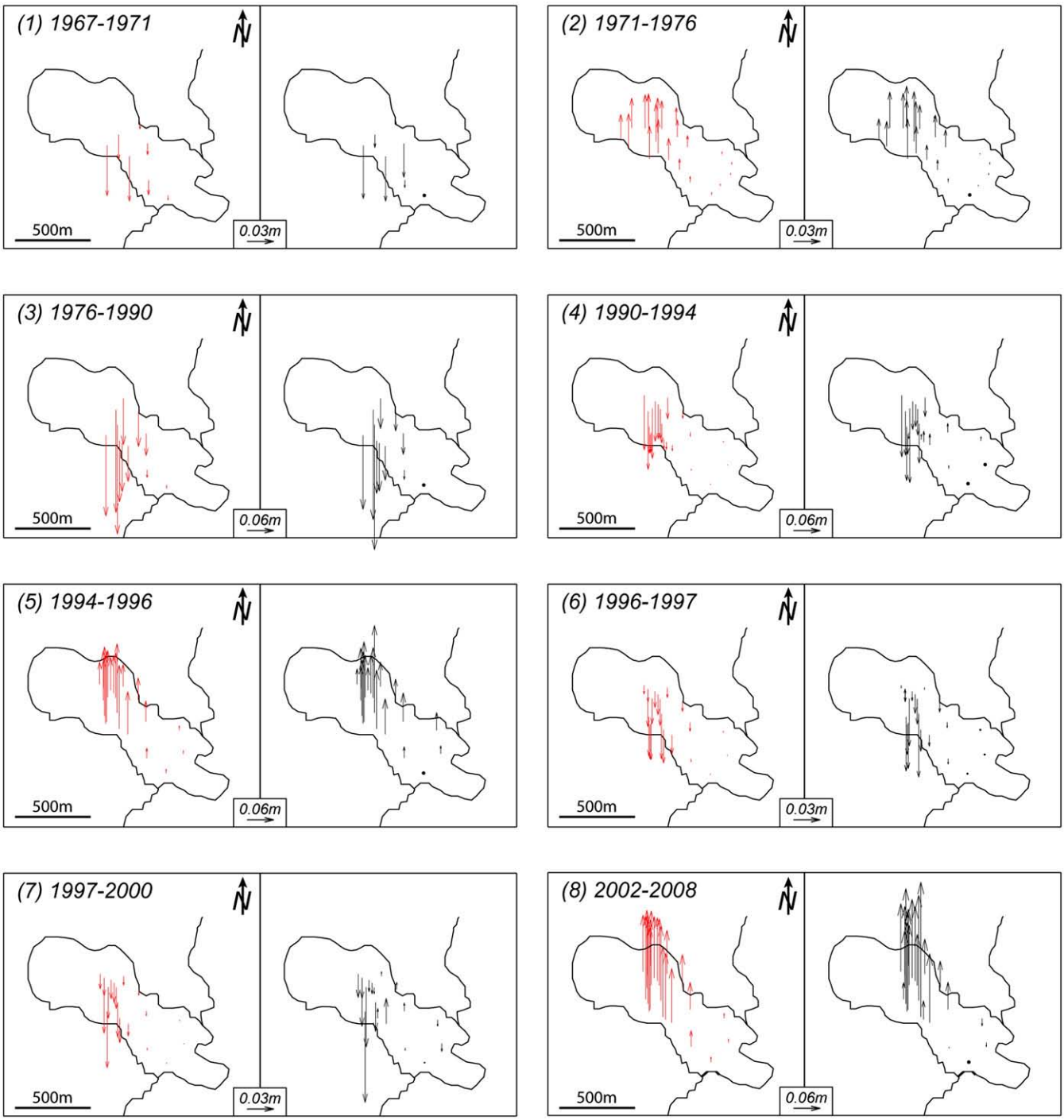

Fig. 9. Comparison between calculated (red) and observed (black) height changes relative to the origin represented as vectors for the eight periods: (1) July 1967–April 1971, (2) April 1971–December 1976, (3) December 1976–November 1990, (4) November 1990–January 1994, (5) January 1994–May 1996, (6) May 1996–December 1997, (7) December 1997–February 2000 and (8) November 2002–May 2008. (For interpretation of the references to color in this figure legend, the reader is referred to the web version of this article.)

Table 1
Summary of the modelled pressure source parameters

Periods	ΔP (MPa)	+−	Radius (m)	+−	X (m)	+−	Y (m)	+−	Depth (m)	+−	ΔV (m³)	Consistency (%)
1967–1971	−2.3	1.2	157	40	2,880,200	75	6,400,067	113	−278	216	-1×10^4	87
1971–1976	1.5	1.3	211	14	2,880,142	68	6,400,262	127	−364	181	1.7×10^4	94
1976–1990	−4.6	1.3	184	40	2,880,190	61	6,400,270	89	−241	146	-3×10^4	97
1990–1994	−5.7	2.1	100	36	2,880,224	82	6,400,326	90	−157	169	-0.6×10^4	64
1994–1996	4.8	1.3	158	40	2,880,208	70	6,400,222	75	−234	174	2.3×10^4	97
1996–1997	−3	1	150	37	2,880,223	60	6,400,209	80	−221	176	-1.2×10^4	81
1997–2000	−4.7	1.4	108	37	2,880,136	62	6,400,221	87	−186	201	-0.7×10^4	65
2002–2008	3.1	1.5	220	35	2,880,222	77	6,400,241	108	−322	158	4×10^4	84

(topography and pressure sources) are modelled using a mesh with triangular elements. Sources of deformation are modelled by pressure changes (ΔP being the change in pressure) in spherical volumes below the crater. We chose to model the pressure sources as spheres and not as sills because the lack of horizontal data do not allow us to well constrain the exact shape of the source (Dieterich and Decker, 1975). Spheres are defined by five parameters: the 3D coordinates of its centre, the dimension of its half axis and ΔP (Peltier et al., 2007).

5.2. Results

The location of the pressure sources that best explain the vertical deformation of the main crater associated with the eight periods previously defined is shown in Fig. 8. The consistency of the modelling is shown in Fig. 9 and Table 1. We are not able to model many of the short-term uplifts and subsidences recorded at less than 3 sites as there is not enough data to constrain the associated sources, so we modelled only the global trend of each period defined in Section 3.2. Between 64% and 97% of the levelling data of the eight periods can be explained by shallow pressure sources, located in a well constrained area below the central sub-crater and extending from a depth of 200–600 m up to the subsurface (Figs. 8–10, Table 1). The location of the inflation sources is very similar from one period to the others, whereas the location of the deflation sources differs slightly (Fig. 8). We plotted on Fig. 10 the parameters of each source with error bars. Even if the depth of pressure sources appears to be within the size of the error bars, their radius and thus their vertical elongation differ (Figs. 8 and 10). The radius of the pressure sources ranged from 100±36 m to 220±36 m, thus the inflation pressure source of the 1971–1976 period reached ~600 m depth whereas the deflation pressure source of the 1990–1994 period reached only about 250 m depth. We distinguished thus three main pressure source depths, as already suggested by Clark and Otway (1989) for the 1976–1982 period: 1) Deep inflation sources extending down to a depth of ~600 m with a radius of ~200 m apparently centred near Donald Mound: 1971–1976, 1994–1996 and 2002–2008 inflation sources (models 2, 5, 8; Figs. 8–10); 2) Shallow deflation sources (180–400 m deep and a radius of 100–150 m) (models 1, 3, 4, 6, 7; Figs. 8–10) located below the central sub-crater; and 3) Very shallow inflation sources generating the short-term cycles of uplift and subsidence recorded only at a few sites between 1979 and 1990.

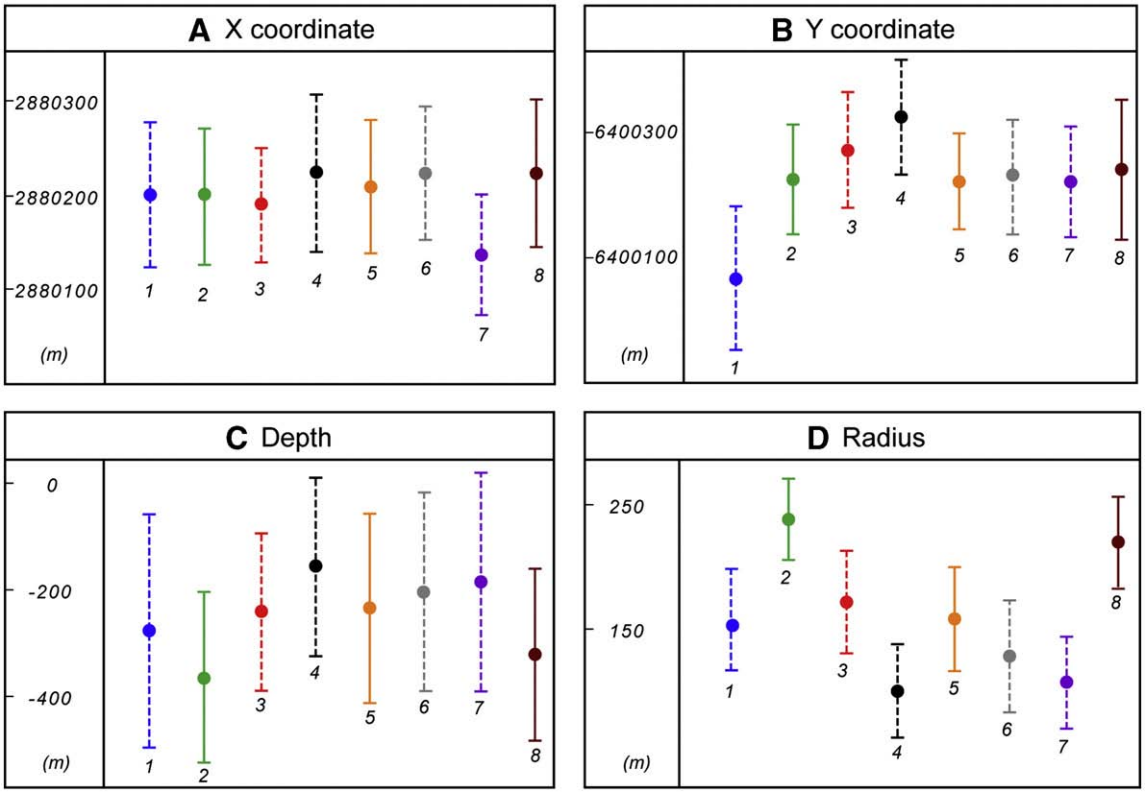

Fig. 10. Parameters of the pressure sources, (A) *X* coordinate, (B) *Y* coordinate, (C) depth of the center, (D) radius, within the error bars modelled for the eight periods: (1) July 1967–April 1971, (2) April 1971–December 1976, (3) December 1976–November 1990, (4) November 1990–January 1994, (5) January 1994–May 1996, (6) May 1996–December 1997, (7) December 1997–February 2000 and (8) November 2002–May 2008. Dotted and continuous lines represent deflation and inflation sources, respectively.

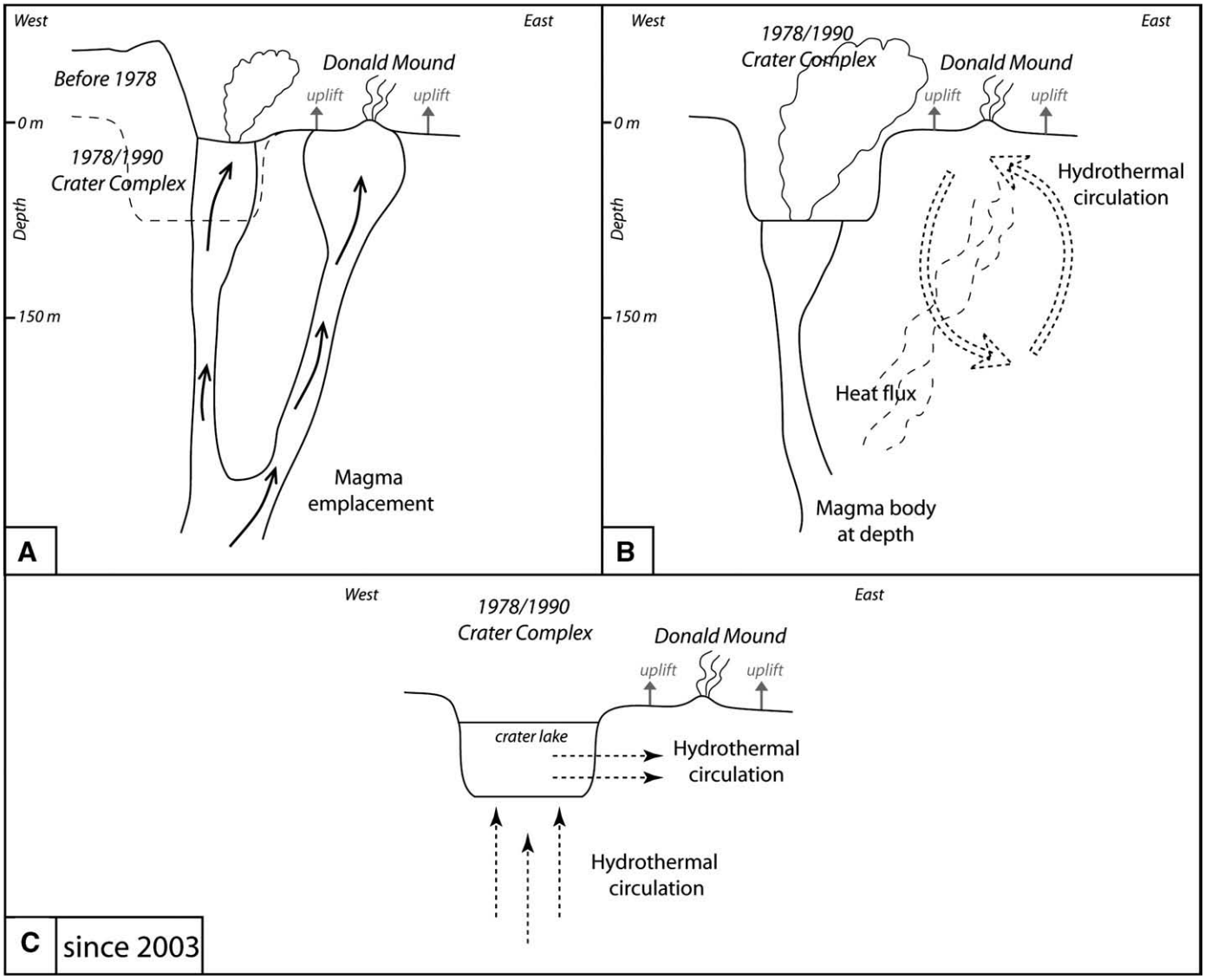

Fig. 11. Schematic sections through the White Island crater representing the three hypotheses advanced to explain uplift episodes: (A) magma emplacement at very shallow depth, (B) hydrothermal circulations, (C) and since 2003, drainage of the lake. The shape of the plumbing system is drawn after Houghton and Nairn (1989) and Nishi et al. (1996a,b).

5.3. Limits

Our investigations are limited by the lack of data in the western sub-crater due to the formation of successive collapse craters in this area. So, not enough data is available to constrain with precision the source extension toward the west and its depth. The monitored area, restricted to the crater, gives us only a minimum depth of the pressure sources but the largest changes recorded within the measured area and the lack of deformation in the eastern part of the crater gives some assurance that pressure sources are shallow (Fig. 5).

Another limitation of our models is the lack of horizontal displacement to constrain the shape of the pressure sources. Finite element models made by Dieterich and Decker (1975) showed that the inversion of only vertical displacement data may provide results that are not unique and that the exact shape of the source cannot be well determined without consideration of vertical and horizontal displacements.

6. Discussion

During the 40 years of levelling monitoring at White Island, successive uplifts and subsidences of the main crater floor have been highlighted. Two main causes can be proposed to explain the inflation and deflation cycles: (1) hydrothermal source (fluid circulations, pressurization/de-pressurization/convection of a sealed hydrothermal fluid reservoir); and (2) magma source (magma intrusions, pressurization/de-pressurization/convection of a shallow magma reservoir) (Fig. 11a, b).

6.1. Origin of the crater uplift episodes

The periods of main crater uplift preceded the resurgences of eruptive activity. These more or less long periods of pre-eruptive uplift signals can be interpreted as due to new input of magma at shallow depth in the volcano somewhere beneath Donald Mound (Fig. 8) as already suggested by Clark and Otway (1989) for the 1971–1976 period. As no relationship exists between the location of the pre-eruptive inflation sources and the 1976–1982 active vents, Clark and Otway (1989) suggested that the inflation was most probably generated by increase of fluid pore pressure in response to heat flux and thermal expansion rather than directly by magma intrusion to shallow depth. Self-potential (SP) surveys carried out in 1993 and 1996 reveal the presence of a well developed volcano-hydrothermal system (Nishi et al., 1996a, 1995). Positive SP anomalies were present over the fumarole areas both in the main crater floor and in the outer slope boarding the main crater. These anomalies, which correlated well with the thermal

anomalies derived from airborne thermal infrared mapping (Mongillo and Wood, 1995), have been interpreted as upflows along the edge of the sub-craters. The inflation sources can be thus explained by the rise of hot fluids from a deeper magma source to shallower levels beneath Donald Mound where they convect through the host rocks to cause thermal expansion. Note that the 1994–1996 crater uplift was not followed by a major eruption as expected by the size of the deformation signal. Accumulated magma at depth during this period might have fed, a few years later, the eruptive period of December 1998–July 2000 which was not preceded by any significant crater uplift (Fig. 3).

The evolution of height changes, magnetic changes, fumarole temperatures and chemistry, previously described (Fig. 7), can all be explained if we suppose that exsolved gases from a magma body were diffused into the hydrothermal system and released to the surface. In consequence we can suppose that the ground uplift that was correlated with high temperatures and peaks in gas concentration was due to a hydrothermal response with an increase of fluid pore pressure in response to heat flow and thermal expansion rather than directly by magma emplacement itself (Fig. 7B). Nishi et al. (1996b) interpreted the shallow earthquakes, mainly originating in the shallow hydrothermal area located beneath the central and eastern sub-craters of the main crater, as resulting from rapid changes in pore fluid pressure.

For the most recent period (2002–2008), another hypothesis involving the drainage of the Crater Lake toward the hydrothermal system (Fig. 11C) can be advanced to explain the uplift centred in the southern part of the central sub-crater (Fig. 5). Just after the formation of the lake in February 2003, the increase of the crater uplift rate was accompanied by an increase in fumarole activity (around pegs C, D and E) and by a 26 m rise of the Crater Lake until 2007 (Fig. 6), suggesting that a significant amount of the volcanic H_2O vapour was condensing into the liquid phase. By contrast, in 2007 a short-term subsidence of the crater floor was accompanied by a drop of the Crater Lake level (Fig. 6). According to Werner et al. (2008) the inflation source could be related to a build up of volatiles in the shallow subsurface due to changes in the permeability structure of the crater following lake filling, and that very little of the magma providing the volatiles was emplaced to permanently reside at shallow depth. A Self Potential (SP) survey in December 2003 revealed a change in the SP anomaly relative to the 1996 survey (Hashimoto et al., 2004; Nishi et al., 1996a). In 1996, a negative SP patch in the middle of the crater floor had been identified by Nishi et al. (1996a) whereas in 2003 a positive zone in the middle-south area had been highlighted by Hashimoto et al. (2004). The change in the SP anomaly distribution between 1996 and 2003 could be attributed to a change in the direction of the ground water supply from/toward the crater lake due to the rise of the lake water level; we can thus suggest a flow from the coast side (east) towards the lake in 1996 and a flow from the lake towards the east in 2003 (Hashimoto et al., 2004). Fluid drainage is favoured along pre-existing fractures, explaining also why the most active fumarole and the peak of uplift are located along the rims delimiting the eastern and the middle sub-craters.

6.2. Origin of the crater subsidence episodes

Crater wide subsidences were recorded during periods of relatively intense eruptive activity (1967–1971, 1979–1990 and 1990–1994 periods, Fig. 8). The ground subsidence can be thus attributed to the continuing removal of magma from depth to feed eruptions at the surface which generate a decrease of pressure and/or volume in depth. The volume variations of the pressure sources found by numerical modelling are in agreement with the low volumes of eruptive materials emitted during the eruptions associated with these deflation periods. The volume variations of the pressure sources during deflation periods were estimated at −0.6 to−3×10^4 m^3 (Table 1), while the volume of emitted products were between 10^4 and 10^5 m^3 for the 1967–1971, 1990–1994, 1996–1997 and 1997–2000 eruptive periods, and was estimated to be 10^7 m^3 for the 1976–1990 period (Houghton and Nairn, 1989; Scott, 1992; Scott et al., 2004). The different locations of the eruptive vents probably explain the slight differences in the location of the modelled deflation source from one period to the other. Superimposed on this behaviour a decompression of the hydrothermal system could also occur. The occasional brief localized inflationary/deflationary episodes during some eruptive sequences (March 1978, May 1980, November 1982, February 1984 and June1987, Fig. 3) would be linked to changes in very shallow heat flows and superficial activity which generated thermal expansion/contraction of the ground in localized areas (commonly the active vent and Donald Mound areas) (see Fig. 2 for location).

Note that following the crater collapse in 1990, subsidence persisted to the west due to continuous material removal associated with the eruption whereas weak uplift was recorded to the east (Fig. 5). Change in the plumbing system just after the crater collapse could have released fluids or magma from a reservoir or subterranean collapse generating uplift in the eastern part of the crater (Otway, 1995, Internal Report GNS).

7. Conclusion

The analysis of 40 years of levelling monitoring at White Island allows us to highlight successive episodes of uplift and subsidence of the main crater. The periods of central sub-crater uplift preceded eruptions or resurgence of eruptive activity, whereas the periods of subsidence accompanied or followed eruptions, indicating a close correlation between ground deformation and eruptive activity. The subsidence during and following eruptions could be linked with removal of material at depth and changes to the hydrothermal system. But as no relationship exists between the locations of the pre-eruptive inflation source and the active vents, we suggested that inflation episodes were most probably generated by the thermal response of the relatively shallow volcano-hydrothermal system to magmatic intrusion, with an increase in fluid pore pressure in response to change of heat and gas flux rather than directly by magma intrusion to shallow depth.

Acknowledgements

Part of this work was supported by grants from the Earthquake Commission of New Zealand (EQC) and the European Commission, 6th Framework Project-'VOLUME', Contract No. 08471. We would like to thank the Buttle family, owners of White Island, for their cooperation. We are grateful to Valérie Cayol and Yo Fukushima for providing the source code and the neighborhood algorithm code. We thank Hugh Bibby, Susan Ellis, Craig Miller and two anonymous reviewers for helpful advices and comments. We also thank Art and Gill Jolly for useful discussions. This is IPGP contribution no. 2470.

References

Cayol, V., 1996. Analyse élastostatique tridimensionnelle du champ de déformations des édifices volcaniques par éléments frontières mixtes. PhD Thesis, Université de Paris VII.

Cayol, V., Cornet, F.H., 1997. 3D mixed boundary elements for elastostatic deformation field analysis. International Journal of Rock Mechanics and Mining Sciences 34 (2), 275–287.

Christoffel, D.A., 1989. Variations in magnetic field Intensity at White Island Volcano related to the 1976–82 eruption sequence. New Zealand Geological Survey Bulletin 103, 109–118.

Clark, R.H., 1970. Volcanic activity on White Island, Bay of Plenty, 1966–69. Part 1. Chronology and crater floor level changes. New Zealand Journal of Geology and Geophysics 13 (3), 565–574.

Clark, R.H., 1973. Surveillance of White Island volcano, 1968–1972. Part 1—volcanic events and deformation of the crater floor. New Zealand Journal of Geology and Geophysics 16, 949–957.

Clark, R.H., 1982. Surveillance of White Island volcano 1972–77: volcanic events and deformation of the crater floor. New Zealand Journal of Geology and Geophysics 25, 317–324.

Clark, R.H., Cole, J.W., 1989. Volcanic monitoring and surveillance at White Island before the 1972–82 eruption sequence. New Zealand Geological Survey Bulletin 103, 9–11.

Clark, R.H., Otway, P.M., 1989. Deformation monitoring associated with the 1976–82 White Island eruption sequence. New Zealand Geological Survey Bulletin 103, 69–84.
Cole, J.W., Nairn, I.A., 1975. Catalogue of the active volcanoes of the world including solfatara fields—Part 22 New Zealand. International Association of Volcanology and Chemistry of the Earth's Interior. 156 pp.
Cole, J.W., Thordarson, T., Burt, R.M., 2000. Magma origin and evolution of White Island (Whakaari) volcano, Bay of Plenty, New Zealand. Journal of Petrology 41 (6), 867–895.
Dieterich, J.H., Decker, R.W., 1975. Finite element modeling of surface deformation associated with volcanism. Journal of Geophysical Research 80 (29), 4094–4102.
Dvorak, J.J., Dzurisin, D., 1997. Volcano geodesy: the search for magma reservoirs and the formation of eruptive vents. Reviews of Geophysics 35 (3). doi:10.1029/97RG00070.
Dzurisin, D., 2003. A comprehensive approach to monitoring volcano deformation as a window on the eruption cycle. Reviews of Geophysics 41 (1). doi:10.1029/2001RG000107.
Dzurisin, D., Yamashita, K.M., Kleinman, W., 1994. Mechanisms of crustal uplift and subsidence at the Yellowstone caldera, Wyoming. Bulletin of Volcanology 56 (261–270).
Fukushima, Y., Cayol, V., Durand, P., 2005. Finding realistic dike models from interferometric synthetic aperture radar data: the February 2000 eruption at Piton de La Fournaise. Journal of Geophysical Research 110 (B03206). doi:10.1029/2004JB003268.
Giggenbach, W.F., Sheppard, D.S., 1989. Variations in the temperature and chemistry of White Island fumarole discharges 1972–1985. New Zealand Geological Survey Bulletin 103, 119–126.
Giggenbach, W.F., Hedenquist, J.W., Houghton, B.F., Otway, P.M., Allis, R.G., 1989. Research drilling into the volcanic hydrothermal system on White Island, New Zealand. EOS 70 (7), 98–102.
Gottsmann, J., Rymer, H., Berrino, G., 2006. Unrest at the Campi Flegrei caldera (Italy): a critical evaluation of source parameters from geodetic data inversion. Journal of Geophysical Research 150 (1–3), 132–145.
Hashimoto, T., et al., 2004. Self-potential studies in Volcanic Areas (5)—Rishiri, Kusatsu-Shirane, and White Island. Journal of the Faculty of Science, Hokkaido University. Series 7, Geophysics 12 (2), 97–113.
Houghton, B.F., Nairn, I.A., 1989. A model for the 1976–82 phreatomagmatic and Strombolian eruption sequence at White Island volcano, New Zealand. New Zealand Geological Survey Bulletin 103, 127–136.
Hurst, A.W., Christoffel, D.A., 1973. Surveillance of White Island volcano, 1968–1972. Part 3—thermo-magnetic effects due to volcanic activity. New Zealand Journal of Geology and Geophysics 16 (4), 965–972.
Hurst, A.W., Rickerby, P.C., Scott, B.J., Hashimoto, T., 2004. Magnetic field changes on White Island, New Zealand, and the value of magnetic changes for eruption forecasting. Journal of Volcanology and Geothermal Research 136, 53–70.
Mongillo, M.A., Wood, C.P., 1995. Thermal infrared mapping of White Island volcano, New Zealand. Journal of Volcanology and Geothermal Research 69, 59–71.
Nishi, Y., Tosha, T., Scott, B.J., Sherburn, S., 1995. Self-potential survey of White Island, Volcano and geothermal observations 1993. Institute of Geological and Nuclear Sciences Report 95/11. Institute of Geological and Nuclear Sciences, Lower Hutt, New Zealand. 34 p.
Nishi, Y., et al., 1996a. Self-potential and audio-magnetotelluric survey in White Island volcano. In: Simmons, S.F., Rahman, M.M., Watson, A. (Eds.), Proceedings of the 18th New Zealand Geothermal workshop, Auckland: University of Auckland, pp. 237–242.
Nishi, Y., Sherburn, S., Scott, B.J., Sugihara, M., 1996b. High-frequency earthquakes at White Island volcano, New Zealand: insights into the shallow structure of a volcano-hydrothermal system. Journal of Volcanology and Geothermal Research 72, 183–197.
Otway, P.M., 1995. Geodetic Observations, 1993; Institute of Geological and Nuclear Sciences Report 95/11. Institute of Geological and Nuclear Sciences Lower Hutt, New Zealand, pp. 26–29.
Peltier, A., Staudacher, T., Bachèlery, P., 2007. Constraints on magma transfers and structures involved in the 2003 activity at Piton de La Fournaise from displacement data. Journal of Geophysical Research 112, B03207. doi:10.1029/2006JB004379.
Sambridge, M., 1999. Geophysical inversion with a neighbourhood algorithm-I. searching a parameter space. Geophysical Journal International 138, 479–494.
Scott, B.J., 1992. White Island Volcano: eruption observations, seismicity and crater geomorphology, 1991. Institute of Geological and Nuclear Sciences Report 92/7. Institute of Geological and Nuclear Sciences, Lower Hutt, New Zealand, pp. 17–23.
Scott, B.J., Manville, V.R., Hancox, G.T., Smith, W.D., Hoverd, J.L., 2004. Assessment of the hazard posed by the Crater Lake, White Island. Institute of Geological and Nuclear Sciences Report 2004/28. Institute of Geological and Nuclear Sciences, Lower Hutt, New Zealand. 34 p.
Werner, C., et al., 2008. Variability of passive gas emissions, seismicity, and deformation during crater lake growth at White Island Volcano, New Zealand, 2002–2006. Journal of Geophysical Research 113 (B01204). doi:10.1029/2007JB005094.
Wicks, C., Thatcher, W., Dzurisin, D., 1998. Migration of fluids beneath Yellowstone caldera inferred from satellite radar interferometry. Science 282, 458–462.